Two magnetic Grüneisen parameters in the ferromagnetic superconductor UGe_2

F. Hardy,[1,2,*] C. Meingast,[1] V. Taufour,[3] J. Flouquet,[3] H. v. Löhneysen,[1,2] R. A. Fisher,[4] N. E. Phillips,[4,5] A. Huxley,[6] and J. C. Lashley[7]

[1]*Forschungszentrum Karlsruhe, Institut für Festkörperphysik, 76021 Karlsruhe, Germany*

[2]*Physikalisches Institut, Universität Karlsruhe, 76128 Karlsruhe, Germany*

[3]*INAC-SPSMS, CEA Grenoble, 38054 Grenoble Cedex, France*

[4]*Lawrence Berkeley National Laboratory, Berkeley, California 94720, USA*

[5]*Department of Chemistry, University of California, Berkeley, California 94720, USA*

[6]*Scottish Universities Physics Alliance, School of Physics, University of Edinburgh, Edinburgh EH9 3JZ, United Kingdom*

[7]*Los Alamos National Laboratory, Los Alamos, New Mexico 87545, USA*

(Received 30 March 2009; revised manuscript received 15 July 2009; published 20 November 2009)

We report ambient-pressure magnetization, heat capacity, and thermal-expansion measurements of the ferromagnetic superconductor UGe_2 in high magnetic fields. An analysis of the magnetic heat capacity derived from both magnetization and specific-heat data shows that UGe_2 is well described in the framework of the molecular-field theory. Our heat-capacity and thermal-expansion results reveal a clear crossover regime, a feature that illustrates the proximity to the quantum critical end point of a first-order boundary between two different ferromagnetic phases. Furthermore, we show that the ferromagnetic contribution to these thermodynamic quantities can be split into two terms with distinct Grüneisen parameters.

DOI: 10.1103/PhysRevB.80.174521 PACS number(s): 74.70.Tx, 71.27.+a, 75.30.Kz, 75.40.Cx

I. INTRODUCTION

The ferromagnet UGe_2 is the first compound that exhibits superconductivity (SC) within its ferromagnetic phase.[1,2] In this material, the transition from ferromagnetism to paramagnetism (PM) at the critical pressure, $p_c \approx 16$ kbar, is first order at zero temperature.[2,3] The emergence of superconductivity is clearly related to an additional boundary, $T_x(p)$, which splits the ferromagnetic phase into a low-pressure FM2 and a high-pressure FM1 region (see Fig. 1). At $T=0$, the transition from FM2 to FM1 is also first order and occurs at a pressure $p_x \approx 12$ kbar where the ordered moment $M_0(p)$ drops from 1.4 to 0.9 μ_B and where the electronic specific-heat coefficient γ (proportional to the effective mass m^* of the quasiparticles) jumps from 50 to about 100 mJ mol^{-1} K^{-2}.[3–7] The sharp discontinuity of the ordered moment, a first-order derivative of the Gibbs energy, is unequivocal proof that the transition is thermodynamic first order. Although it is well established that the transition at p_x is first order at zero temperature with $p_x \approx 12$ kbar, specific-heat anomalies were interpreted both as first order[7] and second order[4] in a narrow pressure range $p_{cr} < p < p_x$ (see Fig. 1). The precise location of p_{cr} is not yet determined exactly.[2–4,8,9] Nevertheless, no discontinuity was detected in neutron scattering, resistivity, magnetization, and NMR/nuclear quadrupole resonance (NQR) measurements below the Curie point at ambient pressure.[2,10] Theoretical works suggest that $T_x(p)$ can arise from a coupling between spin-density wave (SDW) and charge-density wave (CDW) order[11] or, phenomenologically from a peak structure in the electronic density of states.[12]

Furthermore, it was recently suggested that the FM2 region corresponds to a fully polarized state with only a spin-up component because $M(T)$, derived from neutron-scattering measurements, can be fitted in an extended temperature range by an expression given by Stoner.[14] Clearly, more work needs to be done to understand the exact nature of the FM1-FM2 transition. In this article, we present a detailed thermodynamic investigation of UGe_2 at ambient pressure in which we combine magnetization, specific heat, and thermal-expansion measurements up to 8 T.

Our data clearly demonstrate that the change between FM1 and FM2 is a crossover instead of a sharp thermodynamic phase transition in agreement with earlier results. However, the existence of this crossover also clearly indicates that UGe_2, at $p=0$, already feels the proximity of the critical end point (T_{cr}, p_{cr}). We also show that the squared magnetization follows the usual T^2 dependence characteristic of a weak itinerant ferromagnet in the FM2 phase, excluding

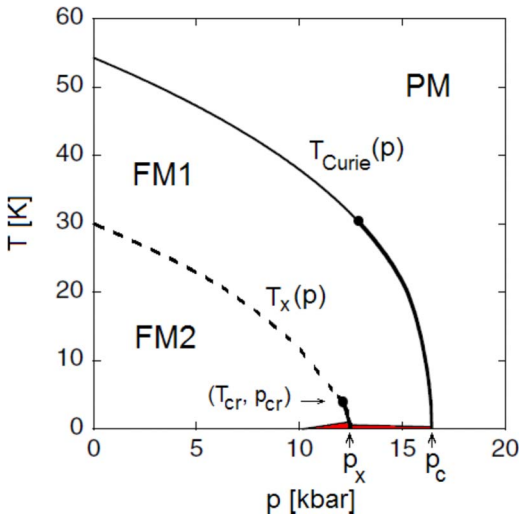

FIG. 1. (Color online) The schematic (p,T) phase diagram of UGe_2 (Ref. 13). Thick lines represent first-order transitions and thin lines denote second-order transitions. The dashed line indicates a crossover while the dots mark the positions of critical points. The superconducting region is represented in red (black area at bottom).

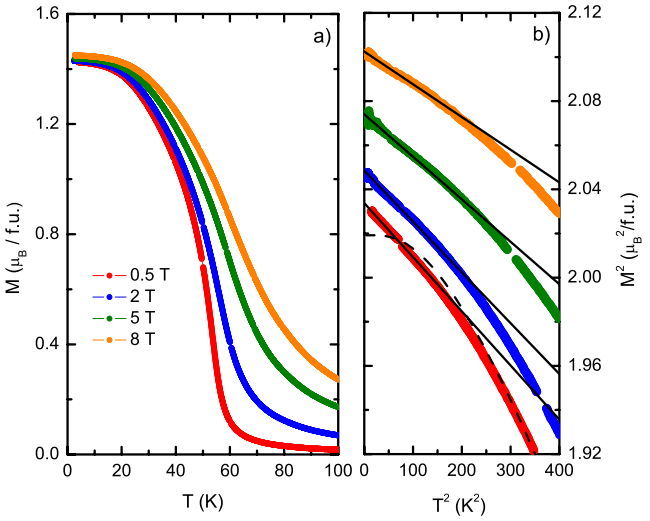

FIG. 2. (Color online) (a) Temperature dependence of the magnetization $M(T)$ of UGe_2 for fields up to 8 T. (b) M^2 as a function of T^2 for temperatures below 20 K. The dashed line is a fit to the Stoner expression $M=M_0(1-\alpha T^{3/2}e^{-\Delta/T})$, using the gap value, $\Delta=40$ K, derived from neutron measurements (Ref. 14).

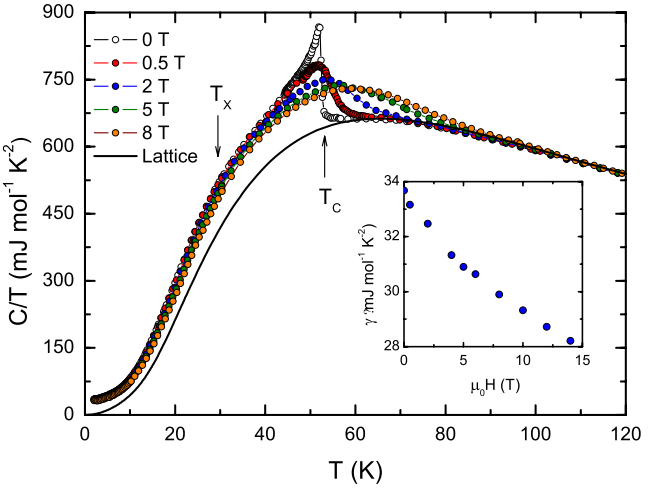

FIG. 3. (Color online) Temperature dependence of C/T of UGe_2 for several fields. The lattice contribution (full line, see Sec. III B 2) is also represented. The inset illustrates the field dependence of the low-temperature linear term γ.

a fully polarized state at low temperature. In addition, the molecular-field approximation (MFA) gives an excellent description of both the specific-heat and thermal-expansion data; a sound test is the ability to extract the phonon contribution to the specific heat.

II. EXPERIMENTAL DETAILS

A parallelepiped-shaped single crystal ($a\times b\times c\approx 3.4\times 1.9\times 0.9$ mm^3) was used in the present experiments. Additional information about the crystal synthesis and the subsequent thermal treatments are given elsewhere.[2] The heat-capacity measurements were performed with the relaxation method using the ^{4}He-PPMS (*physical property measurements system, quantum design*) between 2 and 300 K in magnetic fields up to 8 T. Thermal-expansion measurements were carried out, in the same temperature and field ranges, with a home-built capacitive dilatometer,[15,16] along the a, b, and c axes. The magnetization was determined using the PPMS-vibrating-sample magnetometer option. For all measurements the magnetic field was applied parallel to the easy direction a.

III. EXPERIMENTAL RESULTS AND DISCUSSION

A. Magnetization

Figure 2(a) shows the temperature dependence of the field-cooled magnetization $M(T)$ for several applied magnetic fields above the saturation field which renders the sample monodomain. The ferromagnetic transition at $T_c\approx 55$ K is clearly seen. The signature of T_x is hardly discernible, in contrast with measurements performed at higher pressure, where a phase transition occurs on the $T_x(p)$ line.[14,17] At low temperature, i.e., $T\lesssim T_c/3$, the ordered moment is strongly temperature dependent, and $M^2(T)-M^2(0)$ closely follows the usual T^2 law [Fig. 2(b)]. This law is obeyed for all fields. In the Stoner theory,[18] this low-temperature behavior is characteristic of a weak itinerant ferromagnet for which both spin bands are populated. For comparison, Fig. 2(b) also shows the fit of the 0.5 T data (dashed line) to the Stoner expression $M=M_0(1-\alpha T^{3/2}e^{-\Delta/T})$ for a fully polarized ferromagnet, using a fixed gap value, $\Delta=40$ K, derived from neutron measurements.[14] This fit clearly fails to reproduce the temperature dependence of the magnetization at low temperatures although it describes the data quite well between $\approx$15 and 25 K. It must be pointed out that M decreases only by 1% between 0 and 10 K and this change is well outside the resolution of the neutron measurements. Hence, our results contradict the conclusion of Aso *et al.*[14] that the FM2 region corresponds to a fully polarized state.

B. Heat capacity

Figure 3 shows the measured specific-heat $C(T)$ as a function of temperature for various magnetic fields. As expected, the ferromagnetic anomaly is shifted to higher temperatures and becomes broadened with increasing field. In agreement with previous studies,[2] the signature of the crossover T_x separating the FM1 and FM2 regions is not very pronounced in the raw data at ambient pressure. In the same figure, the solid line represents the estimated phonon background $C_{\rm lat}(T)$ (which is described in more detail in Sec. III B 2), while the inset illustrates the field dependence of the electronic linear term γ. The magnetic (and electronic) heat capacity, $C(T)-C_{\rm lat}(T)$, obtained by subtracting the lattice contribution from the measured specific-heat $C(T)$ is shown in Fig. 4(a): the crossover at T_x is now clearly observed as a broad peak. In the following, we compare this magnetic contribution to the one derived from the magnetization data in the framework of the molecular-field theory.

1. Magnetic specific heat and the molecular-field approximation

In the framework of the MFA, the magnetic heat capacity can be derived from magnetization data. The spins are

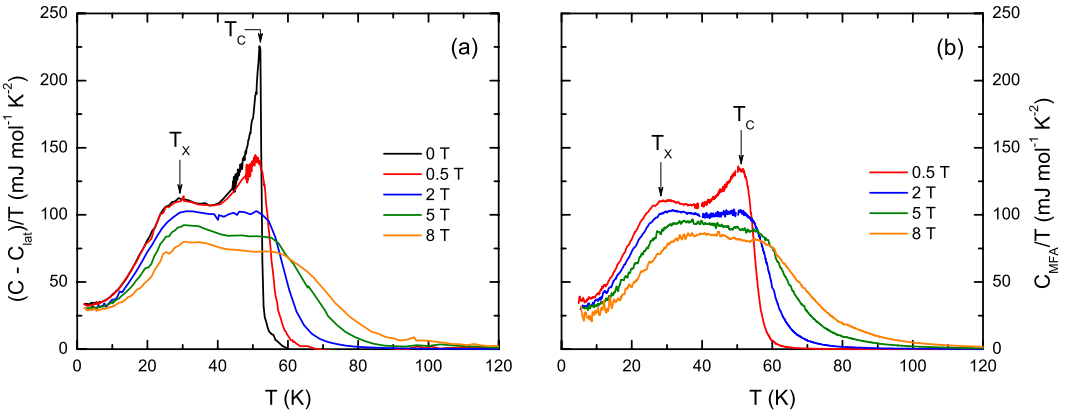

FIG. 4. (Color online) (a) Magnetic and electronic heat capacity obtained by subtracting the lattice contribution C_{lat}/T (see Sec. III B 2) from the measured heat capacity C/T. (b) Magnetic specific heat C_{MFA}/T calculated in the MFA by applying Eq. (1) to the magnetization data.

coupled through a positive exchange interaction via a molecular-field $H_m=\lambda_m M$, where λ_m is the molecular-field constant. This approximation can be applied to itinerant (Stoner model)[18,19] or localized moments (Weiss model). Therefore, in the presence of an applied magnetic field H, the molar magnetic contribution to the specific heat can be written as

$$C_{\mathrm{MFA}}(T) = \underbrace{-\mu_0 V_m \frac{\lambda_m}{2}\left(\frac{\partial M^2}{\partial T}\right)}_{C_M(T)} \underbrace{-\mu_0 V_m H\left(\frac{\partial M}{\partial T}\right)}_{C_H(T)}, \quad (1)$$

where V_m is the molar volume while $C_M(T)$ and $C_H(T)$ are the molecular-field and Zeeman terms, respectively. In most itinerant ferromagnets (such as Co and Fe) this approximation fails because the low temperature decrease in the magnetization is due to spin-wave excitations, which are not taken into account in this simple model. However, UGe_2 is not akin to these familiar 3*d* metals due to its huge uniaxial magnetic anisotropy,[20] and, consequently, longitudinal fluctuations of the magnetization dominate the excitation spectrum.[13] In the low-temperature itinerant FM2 region, the possible excitations are indeed the spin-flip single-particle excitations (Stoner excitations) as observed in the weak itinerant ferromagnet $ZrZn_2$.[21] Hence, this Ising anisotropy together with the relative large ordered moment ($M_0 = 1.4\ \mu_B$) support the relevance of this approximation for UGe_2. Figure 4(b) shows the magnetic specific heat $C_{\mathrm{MFA}}(T)$ obtained by applying Eq. (1) to the magnetization data with a field independent $\lambda_m \approx 155$. The crossover anomaly between the two magnetic regions FM1 and FM2 is clearly visible and corresponds to a broad specific-heat peak. The fact that the magnetic heat capacities displayed in Figs. 4(a) and 4(b) are nearly identical clearly demonstrates that: (i) the anomaly at T_x is of magnetic origin and (ii), the MFA is a good approximation for UGe_2. Surprisingly, even for $T \to 0$, C_{MFA}/T does not tend to zero but to a finite value γ_m which is, within experimental accuracy, equal to the value obtained from the direct measurement of $C(T)$. Consequently, the bare electronic term γ_e must be rather small for UGe_2 at ambient pressure. The existence of a nonzero γ_m confirms that the FM2 region has a delocalized character. Indeed, in the Stoner theory,[18,19] the molecular field causes the splitting of the spin-up and spin-down Fermi surfaces by an amount $\delta\epsilon$ proportional to M. The molecular-field energy $E_M \propto (\delta\epsilon)^2 \propto M^2$. As shown in Sec. III A, $M^2 \propto T^2$ and the low-temperature magnetic heat capacity is proportional to T as $dE_M/dT \propto \gamma_m T$.

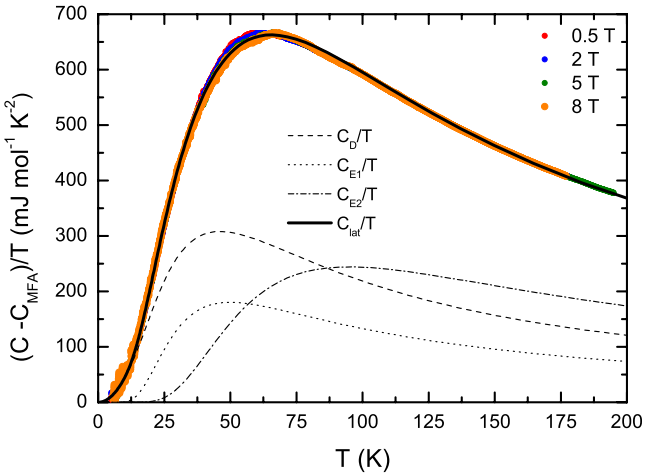

FIG. 5. (Color online) Temperature dependence of $(C - C_{\mathrm{MFA}})/T$ for several magnetic fields. The lattice fit (full line) is also represented together with its Debye (dashed line) and Einstein components (dotted and dash-dotted lines).

The value of λ_m is somewhat smaller than $\frac{T_c}{C_{cw}} \approx 170$ (where C_{cw} is the Curie-Weiss constant) expected for a fully

TABLE I. Fit parameters for the lattice specific heat and volume thermal expansion.

Branch	Θ (K)	p	Γ (10^{-3} kbar^{-1})
Debye (D)	165	3	1
Einstein (E_1)	129	1.8	6.8
Einstein (E_2)	245	4.7	0.3

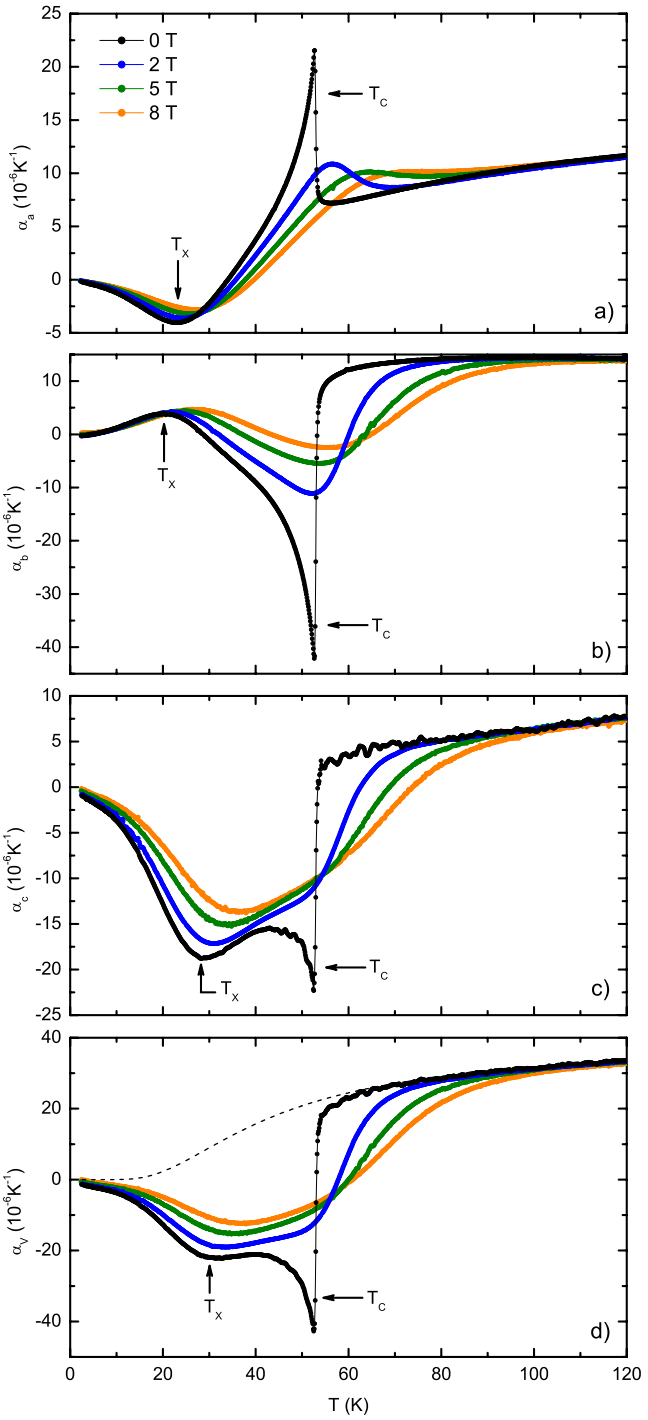

FIG. 6. (Color online) Temperature dependence of the coefficients of linear thermal expansion along the a, b, and c axes and volume for fields up to 8 T. The anomaly at T_x is clearly visible. The lattice contribution for each direction is also shown (dashed line).

localized ferromagnet. This difference, which is just outside the error, can be attributed to $5f$-electron delocalization. The rather weak itinerancy is also corroborated by the value of the magnetic entropy ($S_{\mathrm{mag}}=0.8R\ \ln 2$) which is only 20% lower than $R\ \ln 2$. S_{mag} of UGe_2 is at least twice as large as the entropy observed for the well established itinerant ferromagnets URhGe and UCoGe, which have significantly smaller ordered moments[22,23] (0.4 and 0.07 μ_B, respectively) than that of UGe_2.

2. Lattice heat capacity

The lattice specific-heat $C_{\mathrm{lat}}(T)$ (see Fig. 3) is obtained by subtracting $C_{\mathrm{MFA}}(T)$ from the total specific heat for each magnetic field. As illustrated in Fig. 5, we obtain a lattice contribution $C_{\mathrm{lat}}(T)$ which is field independent; again supporting the validity of the MFA. We analyze $C_{\mathrm{lat}}(T)$ using an empirical model that describes both the acoustic and optical branches of the lattice spectrum. The lattice specific heat is decomposed into a single Debye function $C_D(T)$ and two Einstein terms $C_{E1}(T)$ and $C_{E2}(T)$. The electronic term $\gamma_e T$ is quite small and can be neglected. The model is:

$$C_{\mathrm{lat}}(T) = C_D(p_D, \Theta_D) + \sum_{i=1}^{2} C_{E_i}(p_{E_i}, \Theta_{E_i}), \tag{2}$$

where p_D and p_{E_i} are, respectively, the number of acoustic and optical branches of frequency $\omega_{E_i}=k_B\Theta_{E_i}/\hbar$. In Fig. 5, we show C_{lat}/T for several magnetic fields with the results of fitting the data to Eq. (2) with the restriction $p_D=3$.

The fit parameters are given in Table I. $C_{\mathrm{lat}}(T)$ is very well reproduced by our model over the entire temperature range, confirming that the bare electronic contribution γ_e is indeed negligible. In addition, the energies of the two dispersionless Einstein terms are in good agreement with Born-von Karman calculations, that have revealed the existence of low-lying optical phonons around 10–15 and 20 meV, respectively.[24]

C. Thermal expansion

1. Uniaxial pressure dependences of T_c

In Fig. 6, the three linear expansion coefficients $\alpha_i(T)$ (along the a, b, and c axes) are shown together with the resulting volume expansion α_v as a function of temperature for fields up to 8 T. In zero field, a marked step is observed at T_c for all three directions. These steps are negative in sign along the b and c axis while a positive step is observed along a. The uniaxial and hydrostatic pressure dependences of the Curie temperature are determined using the Ehrenfest relation,

$$\frac{\partial T_c}{\partial p_i} = \frac{V_m \Delta\alpha_i}{\Delta(C/T)}, \tag{3}$$

where the index i refers to the orthorhombic axes and/or to the volume, $V_m=37.34\ \mathrm{cm}^3/\mathrm{mol}$ is the molar volume while $\Delta\alpha_i$ and $\Delta(C/T)$ are the sizes of the anomalies in α_i and C/T, respectively.

The resulting values of $\frac{\partial T_c}{\partial p_i}$ are given in Table II where we also list the corresponding Grüneisen parameters of the FM1 state as

$$\kappa_i \Gamma^i_{FM1} = \frac{1}{T_c}\frac{\partial T_c}{\partial p_i}, \tag{4}$$

where the κ_i's are the uniaxial isothermal compressibilities. Since we do not have the exact values for the κ_i's, we cal-

TABLE II. Uniaxial and hydrostatic pressure dependences of T_c and T_x and Grüneisen parameters for UGe_2 in zero field. The Grüneisen parameters are calculated according to Eqs. (4) and (6).

	a	b	c	v
$\partial T_c/\partial p_i$ (K kbar^{-1})	0.27	−1.05	−0.47	−1.17
$\kappa_i\Gamma^i_{FM1}$ (10^{-3} kbar^{-1})	5	−20	−9	−21
$\partial T_x/\partial p_i$ (K kbar^{-1})	−0.36	0.33	−1	−1.04
$\kappa_i\Gamma^i_{FM2}$ (10^{-3} kbar^{-1})	−13	12	−36	−37

culate the products, $\kappa_i\Gamma^i_{FM1}$ and $\kappa_i\Gamma^i_{FM1}$ (see Sec. III C 3), which nevertheless allows us to compute the ratio of the Grüneisen parameters related to FM1 and FM2.

As illustrated in Fig. 6, the thermal-expansion curves exhibit a large anomaly related to T_x that is very well resolved in comparison with the heat capacity. For a genuine phase transition, as observed at T_c, the three expansivities must exhibit an anomaly at exactly the same temperature. The value of T_x, taken as the position of the extremum of $\alpha_i(T)$, is, however, different for the three directions with deviations of a few kelvin. Therefore, our measurements unambiguously rule out the possibility that T_x corresponds to a thermodynamic phase transition somewhat broadened by sample defects or internal stress at ambient pressure. Thus, the $T_x(p)$ line, observed at large pressures, has to end at a critical pressure p_{cr} where $T_x(p_{cr})=T_{cr}$.

2. Lattice thermal expansion

Using the specific-heats $C_D(T)$, $C_{E1}(T)$, and $C_{E2}(T)$ obtained above (see Table I), the lattice contribution $\alpha_v^{\rm lat}(T)$ to the thermal expansion is estimated by fitting the volume expansion above T_c to the expression

$$\alpha_v^{\rm lat}(T) = \Gamma_D C_D(T) + \Gamma_{E_1} C_{E_1}(T) + \Gamma_{E_2} C_{E_2}(T), \qquad (5)$$

where Γ_D, Γ_{E_1}, and Γ_{E_2} represent Grüneisen-like parameters related to the Debye and the two Einstein temperatures, respectively. These values, also listed in Table I, are the only fit parameters. As shown in Fig. 6, we obtain reasonable lattice expansion coefficients for all axes and the volume.

3. Magnetic contribution to the thermal expansion

The magnetic thermal expansion $\alpha_v^{\rm mag}(T)$, shown in Fig. 7, is obtained by subtracting $\alpha_v^{\rm lat}(T)$ from the measured volume expansion $\alpha_v(T)$. We note that its temperature dependence is very similar to its heat-capacity counterpart. As shown in Fig. 6, the anomalies at T_x and T_c have opposite signs along the a and b axes while the same signs are observed along c and the volume. These opposite behaviors of T_c and T_x with uniaxial stress can be simply explained if the ferromagnetic contribution to $\alpha_i(T)$ consists of two distinct contributions.

Indeed, if the entropy of the system is governed by a single energy scale such as the Fermi-liquid temperature in ordinary metals or the Néel temperature in classical localized antiferromagnets, the thermal expansion is directly proportional to the specific heat. The proportionality constant is the

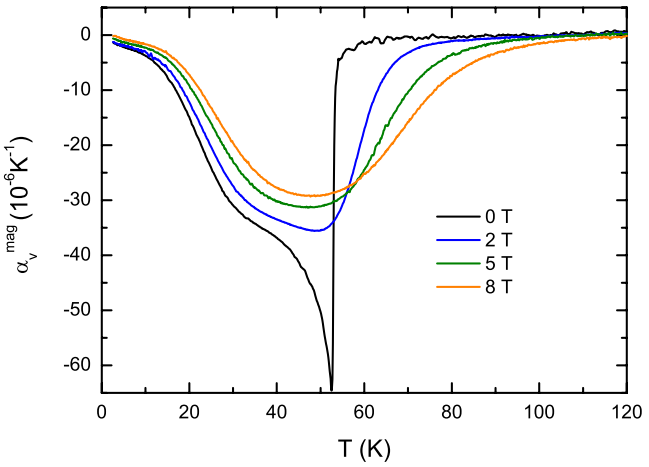

FIG. 7. (Color online) Temperature dependence of the volume magnetic thermal expansion $\alpha_v^{\rm mag}(T)$ for fields up to 8 T.

Grüneisen parameter which is independent of temperature. Figure 8 shows that $C_{\rm MFA}$ is effectively proportional to $\alpha_v^{\rm mag}$ but only in a restricted temperature range below T_x. This clearly indicates that there are two Grüneisen parameters, one being related to FM1 by Eq. (4) and the other to FM2 by

$$\kappa_i\Gamma^i_{FM2} = \frac{1}{T_x}\frac{\partial T_x}{\partial p_i}. \qquad (6)$$

The volume Grüneisen parameter $\kappa_v\Gamma^v_{FM2}$ is equal to -37×10^{-3} kbar^{-1} which is the scale factor between $C_{\rm MFA}$ and $\alpha_v^{\rm mag}$ inferred from Fig. 8 in the low-temperature region. It follows that $\Gamma^v_{FM2}/\Gamma^v_{FM1}\approx 2$ just like T_c/T_x within experimental error. According to Eqs. (4) and (6), we conclude that

$$\frac{\partial T_x}{\partial p} \approx \frac{\partial T_c}{\partial p}, \qquad (7)$$

in the zero-pressure limit. This is in agreement with the pressure-temperature phase diagrams put forward by differ-

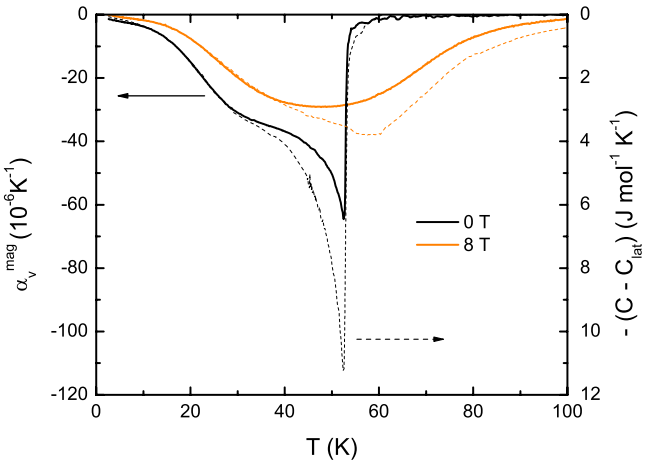

FIG. 8. (Color online) Temperature dependence of the volume magnetic thermal expansion $\alpha_v^{\rm mag}(T)$ (full lines) together with the scaled magnetic specific heat (dashed lines) for 0 and 8 T. We observe that $\alpha_v^{\rm mag}(T)$ is proportional to $C_{\rm MFA}(T)$ only in a restricted temperature range below T_x.

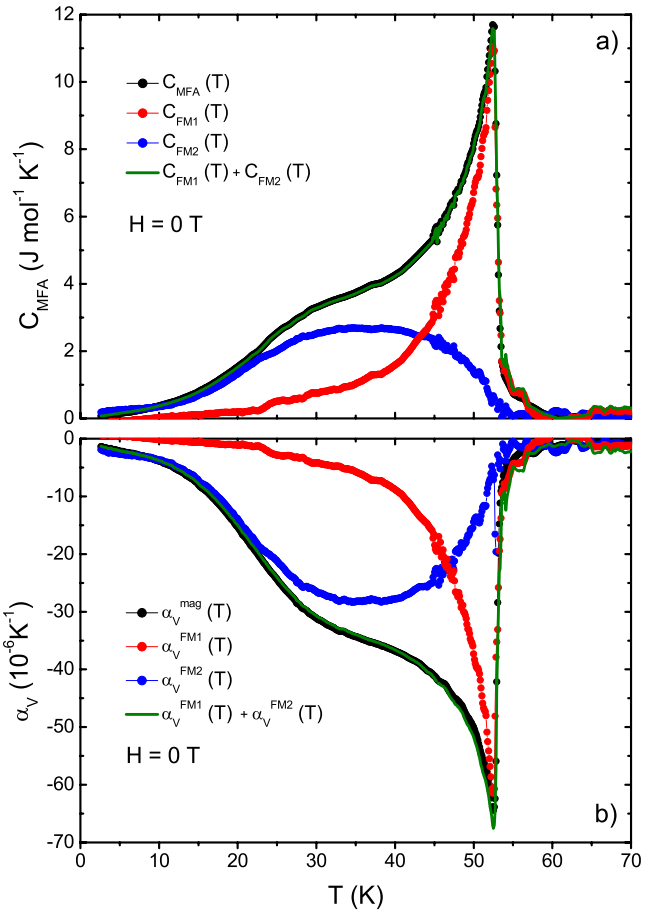

FIG. 9. (Color online) Temperature dependence of the magnetic heat capacity (a) and magnetic thermal expansion (b) in zero field. These two quantities are decomposed into two contributions related to FM1 (red) and FM2 (blue).

ent authors[25,26] and thus confirms the consistency of our analysis.

IV. DISCUSSION

The existence of two distinct energy scales implies that the magnetic heat capacity and thermal expansion can be written as the sum of two contributions,

$$C_{\mathrm{MFA}}(T) = C_{FM1}(T) + C_{FM2}(T),$$
$$\alpha^{v}_{\mathrm{mag}}(T) = \underbrace{\Gamma^{v}_{FM1} \cdot C_{FM1}(T)}_{\alpha^{v}_{FM1}(T)} + \underbrace{\Gamma^{v}_{FM2} \cdot C_{FM2}(T)}_{\alpha^{v}_{FM2}(T)}, \qquad (8)$$

where $C_{FM1}(T)$ and $C_{FM2}(T)$ are the specific heats related to FM1 and FM2, respectively. This simple decomposition is valid if Γ^{v}_{FM1} and Γ^{v}_{FM2} are temperature independent. By solving this system of equations, we obtain the curves given in Fig. 9. The red curves are directly related to the onset of ferromagnetism at T_c. The Grüneisen parameter derived from the ratio of these two curves gives $\frac{\partial T_c}{\partial p}$. Interestingly, the contribution related to FM2 (blue curves) sets in just at T_c as if it was triggered by the onset of ferromagnetic order. It then develops a maximum at T_x and finally leads to the low-temperature linear terms in $C(T)$, $\alpha(T)$ and M^2 vs T^2. Thus, the Grüneisen parameter derived by the ratio of the blue curves provides $\frac{\partial T_x}{\partial p} \propto \frac{\partial \gamma}{\partial p}$.

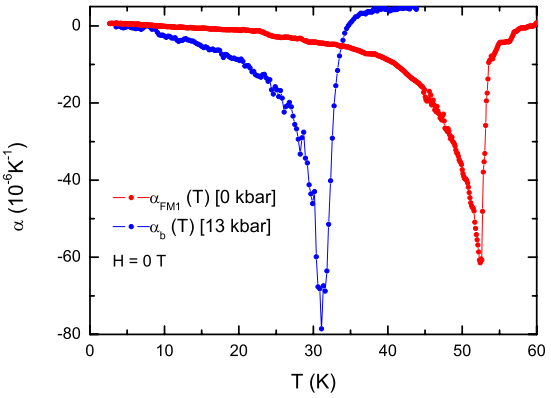

FIG. 10. (Color online) Temperature dependence of the ambient-pressure FM1 magnetic thermal expansion. It is compared to the thermal expansion measured along the b axis at 13 kbar (Ref. 27). Because of its small lattice contribution, $\alpha_b(T)$ is almost entirely of magnetic origin.

To corroborate our analysis, we compare $\alpha^{v}_{FM1}(T)$ with thermal-expansion measurements performed at 13 kbar (using a strain gauge),[27] i.e., above the critical pressure p_x at which the FM2 state collapses (see Fig. 10). Although shifted due to the pressure dependence of T_c, these two curves have a very similar behavior (i.e., no hump related to FM2). This indicates that only the FM1 (red) contribution persists above p_x and that $\gamma(p)$ no longer increases above this pressure. This is consistent with specific-heat measurements $C(p,T)$ under pressure, which shows that $\gamma(p)$ increases with pressure and levels off above p_x at a value of $\gamma_{FM1}(p>p_x) \approx 100$ mJ mol^{-1} K^{-2}.[5] In addition, our results are compatible with magnetization measurements under pressure (for $p > p_x$)[17] which reveal that FM1 is distinguished from FM2 by (i) a smaller magnetic moment M_0=0.9 μ_B, (ii) a huge increase in the magnetic anisotropy, and (iii) a flatter temperature dependence of the low-temperature magnetization.

Our results indicate that the linear terms of $C(T)$, $\alpha(T)$, and the T^2 dependence of M^2 have a common $5f$ electronic origin in the FM2 region. On the other hand, the large value of γ observed in the FM1 phase, which develops from the suppression of FM2, appears not to have the same origin (mainly changes in band mass renormalization and not in the spin fluctuation dynamics) as shown by the weak value of the linear term in $\alpha(T)$ related to the very low-pressure dependence of γ. Further specific-heat and thermal-expansion measurements extended above the critical pressure p_c, where ferromagnetism vanishes, would be useful.

V. CONCLUSIONS

From magnetization data, we find that, at ambient pressure, the itinerant phase FM2 of UGe_2 does not correspond to a fully polarized state for which only one spin direction contributes to the magnetic polarization. We have demonstrated that the magnetic and thermodynamic properties of

UGe_2 can be understood in the simple context of the molecular-field theory. Based on a detailed analysis, the lattice and magnetic contributions to the specific heat and the thermal expansion were determined. Moreover, we confirm that T_x is not the signature of a thermodynamic phase transition as it is the case at T_{Curie}. Thus, the first-order $T_x(p)$ line ends at a critical end point (T_{cr}, p_{cr}) while the zero temperature limit is reached at p_x. In addition, the change from FM1 to FM2 upon cooling is clearly given by the magnetic properties of the uranium $5f$ electrons. The open question is whether this change is driven by changes in the degree of localization of these heavy quasiparticles. Similarly to the pressure-induced superconductor $CeIn_3$,[28] superconductivity, in UGe_2, is observed at the point where the FM2 phase collapses, *i.e.*, where, at least, changes of the Fermi surface have been detected.[29] In order to distinguish between band-structure and correlation effects, a careful determination of the superconducting phase diagram on crossing the (T_x, p_x) first-order line is required. UGe_2 appears as a perfect example for the studies of quantum critical end points as it is now highly discussed for valence transitions[30] and metamagnetic transitions in ferromagnets and antiferromagnets.[31–33]

ACKNOWLEDGMENTS

This work was supported by the Helmholtz-Gemeinschaft (Virtual Institute of Research on Quantum Phase Transitions Project No. VH-VI-127) and the Deutsche Forschungsgemeinschaft under Grant No. FOR 960. Work at LBNL was supported by the Director, Office of Science, Office of Basic Energy Sciences, of the U.S. Department of Energy under Contract No. DE-AC02-05CH11231.

*frederic.hardy@ifp.fzk.de

[1] S. S. Saxena *et al.*, Nature (London) **406**, 587 (2000).
[2] A. Huxley, I. Sheikin, E. Ressouche, N. Kernavanois, D. Braithwaite, R. Calemczuk, and J. Flouquet, Phys. Rev. B **63**, 144519 (2001).
[3] C. Pfleiderer and A. D. Huxley, Phys. Rev. Lett. **89**, 147005 (2002).
[4] N. Tateiwa, T. C. Kobayashi, K. Amaya, Y. Haga, R. Settai, and Y. Ōnuki, Phys. Rev. B **69**, 180513(R) (2004).
[5] N. Tateiwa, T. C. Kobayashi, K. Amaya, Y. Haga, R. Settai, and Y. Ōnuki, Physica B **312-313**, 109 (2002).
[6] R. A. Fisher, F. Bouquet, J. C. Lashley, N. E. Phillips, A. Huxley, and J. Flouquet, Bull. Am. Phys. Soc. **48**, 922/R1.026 (2003).
[7] F. Bouquet, R. A. Fisher, F. Hardy, J. C. Lashley, N. E. Phillips, A. Huxley, and J. Flouquet (unpublished).
[8] N. Tateiwa, T. C. Kobayashi, K. Hanazono, K. Amaya, Y. Haga, and Y. Ōnuki, J. Phys.: Condens. Matter **13**, L17 (2001).
[9] H. Kotegawa *et al.*, J. Phys. Soc. Jpn. **74**, 705 (2005).
[10] H. Kotegawa *et al.*, J. Phys.: Condens. Matter **15**, S2043 (2003).
[11] S. Watanabe and K. Miyake, J. Phys. Soc. Jpn. **71**, 2489 (2002).
[12] K. G. Sandeman, G. G. Lonzarich, and A. J. Schofield, Phys. Rev. Lett. **90**, 167005 (2003).
[13] A. D. Huxley, S. Raymond, and E. Ressouche, Phys. Rev. Lett. **91**, 207201 (2003).
[14] N. Aso, G. Motoyama, Y. Uwatoko, S. Ban, S. Nakamura, T. Nishioka, Y. Homma, Y. Shiokawa, K. Hirota, and N. K. Sato, Phys. Rev. B **73**, 054512 (2006).
[15] R. Pott and R. Schefzyk, J. Phys. E **16**, 444 (1983).
[16] C. Meingast, V. Pasler, P. Nagel, A. Rykov, S. Tajima, and P. Olsson, Phys. Rev. Lett. **86**, 1606 (2001).
[17] A. Huxley, E. Ressouche, B. Grenier, D. Aoki, J. Flouquet, and C. Pfleiderer, J. Phys.: Condens. Matter **15**, S1945 (2003).
[18] E. C. Stoner, Proc. R. Soc. London, Ser. A **165**, 372 (1938).
[19] E. C. Stoner, Proc. R. Soc. London, Ser. A **169**, 339 (1939).
[20] T. Sakon, S. Saito, K. Koyama, S. Awaji, I. Satoh, T. Nojima, K. Watanabe, and N. K. Sato, Phys. Scr. **75**, 546 (2007).
[21] E. A. Yelland and S. M. Hayden, Phys. Rev. Lett. **99**, 196405 (2007).
[22] N. T. Huy, A. Gasparini, J. C. P. Klaasse, A. de Visser, S. Sakarya, and N. H. van Dijk, Phys. Rev. B **75**, 212405 (2007).
[23] N. T. Huy, D. E. de Nijs, Y. K. Huang, and A. de Visser, Phys. Rev. Lett. **100**, 077002 (2008).
[24] S. Raymond and A. Huxley, Phys. Rev. B **73**, 094420 (2006).
[25] Y. Haga, M. Nakashima, R. Settai, S. Ikeda, T. Okubo, S. Araki, T. C. Kobayashi, N. Tateiwa, and Y. Ōnuki, J. Phys.: Condens. Matter **14**, L125 (2002).
[26] Y. Kitaoka *et al.*, J. Phys.: Condens. Matter **17**, S975 (2005).
[27] V. Taufour (private communication).
[28] R. Settai *et al.*, J. Phys. Soc. Jpn. **74**, 3016 (2005).
[29] T. Terashima, T. Matsumoto, C. Terakura, S. Uji, N. Kimura, M. Endo, T. Komatsubara, and H. Aoki, Phys. Rev. Lett. **87**, 166401 (2001).
[30] S. Watanabe, A. Tsuruta, K. Miyake, and J. Flouquet, Phys. Rev. Lett. **100**, 236401 (2008).
[31] J. Flouquet, Prog. Low Temp. Phys. **15**, 139 (2005).
[32] T. Misawa, Y. Yamaji, and M. Imada, J. Phys. Soc. Jpn. **78**, 084707 (2009).
[33] D. Belitz, T. R. Kirkpatrick, and J. Rollbuhler, Phys. Rev. Lett. **94**, 247205 (2005).